Charge-Carrier Trapping Dynamics in Bismuth-Doped Thin Films of $MAPbBr_3$ Perovskite

Aleksander M. Ulatowski, Adam D. Wright, Bernard Wenger, Leonardo R.V. Buizza, Silvia G. Motti, Hannah J. Eggimann, Kimberley J. Savill, Juliane Borchert, Henry J. Snaith, Michael B. Johnston, and Laura M. Herz*

Department of Physics, University of Oxford, Clarendon Laboratory, Parks Road, Oxford OX1 3PU, United Kingdom

E-mail: laura.herz@physics.ox.ac.uk

Abstract

Successful chemical doping of metal halide perovskites with small amounts of heterovalent metals has attracted recent research attention because of its potential to improve long-term material stability and tune absorption spectra. However, some additives have been observed to impact negatively on optoelectronic properties, highlighting the importance of understanding charge-carrier behaviour in doped metal-halide perovskites. Here, we present an investigation of charge-carrier trapping and conduction in films of $MAPbBr_3$ perovskite chemically doped with bismuth. We find that the addition of bismuth has no effect on either the bandgap or exciton binding energy of the $MAPbBr_3$ host. However, we observe a substantial enhancement of electron-trapping defects upon bismuth doping, which results in an ultrafast charge-carrier decay component, enhanced infrared emission and a notable decrease of charge-carrier mobility. We propose that such defects arise from the current approach to Bi-doping through addition of $BiBr_3$, which may enhance the presence of bromide interstitials.

Graphical TOC Entry

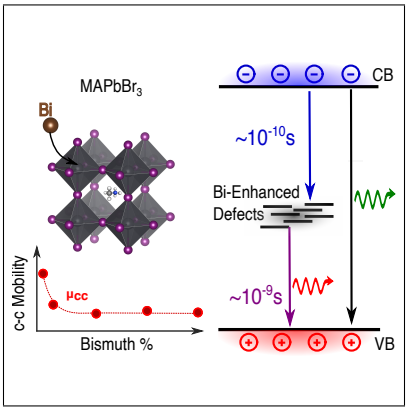

Keywords

Bismuth doping, $MAPbBr_3$ perovskite, charge-carrier dynamics, decreased mobilities, IR photoluminescence, defect formation, trap enhancement, THz photoconductivity, PL quenching

Rapid advances in the field of lead halide perovskite semiconductors over the last decade have resulted in highly efficient perovskite-based solar cells, currently exceeding 25% power conversion efficiency (PCE).[1] Such impressive progress lies in the extraordinary properties of these materials: low exciton binding energies,[2–4] high charge-carrier mobilities,[5–7] low densities of mainly shallow traps[8] and the resulting relatively long diffusion lengths of charge carriers.[7] Another attractive feature of metal halide perovskites is their wide bandgap tunability, e.g. through halide substitution.[9] To further improve the properties of the active layer, heterovalent doping of the perovskite crystal with bismuth has been investigated in multiple studies.[10–19] All of the experimental studies followed the same procedure of doping $MAPbBr_3$ single crystals with bismuth ions through the addition of $BiBr_3$ salt to the precursor solution, as described by Abdelhady et al.[10] This method was shown to efficiently incorporate bismuth into the perovskite structure by lead substitution (because of the similarity of ionic radii and electronic structure), as indicated by plasma and flame spectroscopy of Bi-doped single crystals of $MAPbBr_3$ perovskites.[10,11] Early results indicated positive effects of bismuth additive on the properties of the crystals, such as prolonged stability of inorganic, caesium-based perovskites,[13] a rise of electrical conductivity upon bismuth doping of single crystals of $MAPbBr_3$,[10,11] improved visible-light absorption,[12] and changes in the absorption spectrum initially identified as bandgap tuning by Abdelhady et al.[10] However, some investigations have also reported that the addition of bismuth to the perovskite crystal has negative effects on the optoelectronic properties of the semiconductor.[14–17] Subsequent studies of $MAPbBr_3$ crystals revealed an increase of within-gap trap states upon bismuth addition and showed the invalidity of the bandgap tuning effect.[11,14,18,19] Such additional traps have also been shown to decrease the performance of the solar cells upon bismuth doping of a mixed-cation, lead mixed-halide perovskite active layer.[17] However, the mechanisms by which bismuth affects the optoelectronic properties of perovskites are still poorly understood, with only a few reports on the topic having been published in recent years.[11,15,17,18] Such

an understanding will be critical to the evaluation of the positive and negative trade-offs for chemical doping of metal halide perovskites with heterovalent metals, and will further our general understanding of how different additives may alter the properties of these materials.

In this study, we have investigated the effects of chemical doping of $MAPbBr_3$ perovskite thin films with bismuth. We employed a variety of techniques, including photoluminescence (PL) and absorption measurements, as well as time-resolved, ultrafast THz photoconductivity studies, to examine the energetics and dynamics of bismuth-induced charge-carrier trapping in films of different doping levels. We observe an increased density of mid-bandgap, luminescent trap states as well as a rise of energetic disorder upon bismuth doping of $MAPbBr_3$, by examining steady-state absorption and emission spectra of the thin films. We note that the presence of these traps leads to faster recombination of photoexcited charge-carriers, as evident from the significant reductions in band-edge photoluminescence and THz photoconductivity lifetimes. We also report a significant decrease of the charge-carrier mobility when bismuth is added to the films, in accordance with the accompanying rise in energetic disorder. Finally, we deduce that ultrafast trapping of electrons contributes significantly to the worsening of the optoelectronic properties, as indicated by the time-dependent dynamics of the THz photoconductivity. Therefore, the addition of bismuth leads to a significant rise in trap-state density and energetic disorder that manifests itself in quenched PL, lowered charge-carrier mobility and extended band tails below the absorption onset.

We begin our investigation through a careful analysis of the steady-state absorption spectra of thin films of bismuth-doped $MAPbBr_3$. Figure 1 displays absorption spectra for a range of bismuth dopant percentages corresponding to the concentration of bismuth salt in the precursor solution, as outlined in the SI. The observed changes in the absorption spectra of Bi-doped $MAPbBr_3$ films include an apparent redshift of the absorption onset, together with a decreased height of the excitonic peak with increased bismuth content. In order to examine the origin of these changes we note that the absorption spectrum of a semiconductor has both excitonic and free electron-hole contributions, both of which are broadened due to

energetic disorder, electron-phonon interactions and natural broadening.[20–23] While both bound excitonic and free species contribute to the continuum absorption above the band edge, the pronounced peak below the band gap is caused by the ground state of bound excitonic states alone.

To understand why bismuth doping causes the observed decrease of the sub-gap excitonic peak intensity requires detailed examination of the absorption onset according to the theory by Elliott.[20] In general, such changes could originate either from a reduction in the strength of bound excitonic transitions because of a decrease in the exciton binding energy, or from an increased broadening of the spectrum, which reduces the maximum intensity of the exciton peak through spectral spreading of the excitonic oscillator strength.[24] While a reduction in excitonic binding energy will lead to an apparent blueshift of the absorption offset, spectral broadening will conversely cause the presence of extended sub-gap tails resulting from increased energetic disorder. It is therefore apparent from Figure 1 that the latter applies, but to confirm this and dispel the previous notion of a doping-induced band shift,[10] we carried out a full modelling of the absorption onset with Elliott theory to distinguish clearly between such effects.[24] This Elliott analysis has been previously applied to undoped metal halide perovskites[21,24] in order to reveal information about the bandgap of the semiconductor E_{g} and the exciton binding energy E_{b}, as well as the broadening of the absorption spectrum (characterised by Γ as explained in the SI) associated with energetic disorder.

The inset to Figure 1 displays as solid lines fits to the absorption onset of bismuth-doped $MAPbBr_3$ films, based on the theory by Elliott[20] and outlined in Section 2.2 in the SI. The extracted fitting parameters are listed in Table 1 and reveal a significant increase in the broadening (Γ) of the absorption spectrum with increasing bismuth doping. Importantly, the exciton binding energy is essentially unchanged across the range of Bi concentrations investigated, and the spectra are well described by a single value of bandgap energy E_{g}, here globally optimised for all samples. Although the initial report by Abdelhady et al. con-

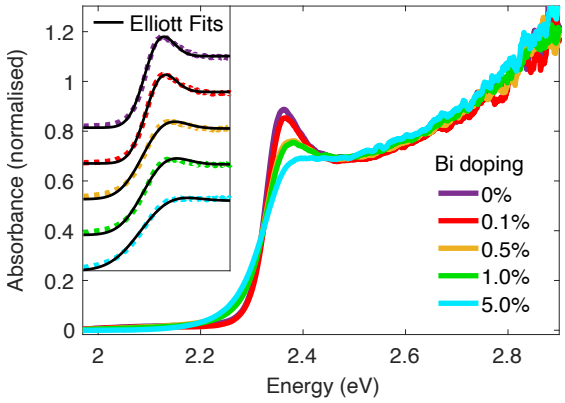

Figure 1: The absorbance (negative base-10 logarithm of transmittance) of $MAPbBr_3$ thin films with different bismuth doping levels. The inset shows Elliott fits plotted in black on top of the experimental data for the energy range 2.2 eV-2.5 eV, offset vertically for each sample for better visibility. The parameters obtained from the fits are shown in Table 1. Full details of the fitting procedure can be found in the SI.

Table 1: Fitting parameters obtained from Elliott fits to the absorption onset spectra of Bi-doped $MAPbBr_3$ films shown in the inset of Figure 1. The bandgap energy E_g was optimised globally for all samples, with exciton binding energy E_b and broadening parameter Γ left as free parameters for each doping concentration.

Bi doping	E_b (meV)	E_g (eV)	Γ (meV)
0%	34.8	2.38	30.1
0.1%	33.3	2.38	30.7
0.5%	33.3	2.38	42.7
1.0%	32.6	2.38	43.7
5.0%	33.5	2.38	55.1

cluded that bandgap narrowing occurs upon bismuth doping,[10] our results clearly indicate that the effect of bismuth is in fact limited to a broadening of the absorption onset due to energetic disorder, in agreement with previous reports investigating single crystal absorption via sensitive ellipsometry measurements.[14] Our detailed Elliott fits further prove that intrinsic parameters such as exciton binding energy and band gap energy are unaffected by Bi-doping of $MAPbBr_3$, making the observed changes an entirely extrinsic effect.

To further investigate whether the increase in energetic broadening with bismuth doping may be correlated with the introduction of additional defect states, we recorded steady-state photoluminescence spectra from photoexcited films. Figure 2 reveals that for $MAPbBr_3$ thin films measured in vacuum, bismuth doping leads to a quenching of the band-edge PL emission, a small blueshift of this emission peak (shifting by about 10 nm across the sample set), as well as a significant enhancement of an infrared (IR) emission band associated with radiative recombination of charge carriers from states within the band gap. The observation of the band-edge PL blueshift reinforces the conclusion that no bandgap narrowing occurs upon bismuth doping of the perovskite crystal. The observed blueshift is instead most likely associated with lowered photon reabsorption in the doped films,[18,25] given that bismuth doping induces faster charge-carrier trapping (see below), and therefore carriers generated initially nearer the front surface have insufficient time to diffuse deeper into the bulk of the thin film.

To examine the origin of the observed below-gap infrared PL emission band, we note that PL spectra measured in air and shown in Figure S1 in the Supporting Information clearly reveal this band to be present for both the bismuth doped films as well as the undoped material, although its intensity is considerably stronger in the former. This observation suggests that the trapping mechanism is not exclusively caused by the chemical bismuth doping, but rather originates from traps that can generally be present in $MAPbBr_3$ and are strongly enhanced through the bismuth-doping process. Motti et al.[26] previously investigated such broadband IR emission from $MAPbBr_3$ perovskites in the absence of bismuth doping and

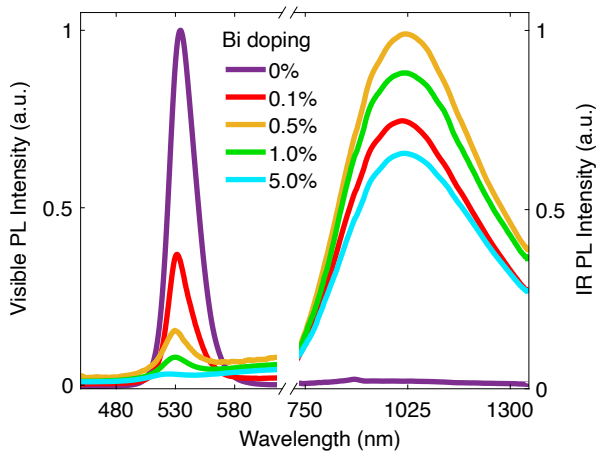

Figure 2: PL spectra of Bi-doped $MAPbBr_3$ thin films photoexcited at 400 nm, measured in vacuum. The band-edge emission can be seen at 530 nm and the sub-bandgap emission band from trap states at around 1000 nm. Significant quenching of the band-edge PL with bismuth doping can be observed, together with an overall enhancement of IR emission in the doped films. The relative intensities of the IR to visible peaks are arbitrary.

found it to be associated with the recombination of charge carriers trapped by native point defects in the crystal structure. Their work identified electron-trapping defects originating from lead vacancies and halide interstitials as the cause of the IR emission, based on density functional theory (DFT) calculations and analysis of the dynamics of charge-carrier trapping in $MAPbBr_3$ films interfaced with either hole- or electron-extraction layers. Since for the case of Bi-doped $MAPbBr_3$ films under investigation here, the intensity of such IR emission is enhanced following bismuth doping, we propose that the preparation pathway of these bismuth-doped materials leads to enhanced electron traps of a similar origin, although a new defect band directly attributable to bismuth cannot be entirely excluded as a cause.[16]

The observed energetic disorder and enhanced trap-state emission upon bismuth doping of $MAPbBr_3$ perovskites may be linked with the short lifetimes of photoluminescence observed for bismuth-doped $MAPbBr_3$.[11,15,18] To investigate such correlations, we further analyse the charge-carrier dynamics in these bismuth-doped perovskite films. We examine the temporal behaviour of the photoluminescence using the time-correlated single photon counting (TCSPC) technique (details given in SI). The decay of the band-edge photolumi-

nescence displayed in Figure 3 shows a shortening of the PL lifetimes in the bismuth-doped films compared to the pristine perovskite, to time scales that are limited by the response of the detector (shown in Figure S2 in the SI). Therefore, the lack of variation of PL lifetimes between films with different doping levels likely originates from the limited time resolution of the measurement. In the inset of Figure 3, we contrast the dynamics of the band-edge emission with those observed for the below-gap, broad IR emission band, for the 0.1% bismuth-doped $MAPbBr_3$ film. Similar to previous observations for $MAPbBr_3$ perovskite in the absence of bismuth doping,[26] the IR emission transient exhibits a slowly rising onset and a relatively long lifetime. The slow rise matches the timescale of the decay of the band-edge emission, suggesting that the population of charge-carriers emitting in the IR is fed by trapping of free charge-carriers emitting just below the band edge. It is also evident that this electron trapping mechanism makes a significant contribution to the overall decay of the photoexcited charge-carrier population. Overall, these transients support the hypothesis that the enhanced IR emission in the doped films is caused by the selective trapping of electrons and their subsequent radiative recombination with free holes.

As the next step, we examined the dynamics of the photoexcited charge carriers with higher temporal resolution, employing the Optical-Pump THz-Probe (OPTP) technique, as described previously by Wehrenfennig et al.[6] and outlined in the SI. This approach allows the recording of the time-resolved THz photoconductivity following excitation with short (35 fs) laser pulses for a range of fluences, as shown in Figure 4 for $MAPbBr_3$ films with bismuth doping levels of 0%, 0.1% and 5%. Since the measured photoconductivity of the sample is proportional to the charge-carrier density, OPTP is a direct, non-contact probe of the photoexcited charge-carrier population in the perovskite thin films.

As previously described by Herz,[27] in hybrid perovskites, the room-temperature decay dynamics of a charge-carrier population (n_{cc}) after photoexcitation mostly depend on the contribution from three recombination pathways: monomolecular (trap-assisted) recombination with rate k_1, bimolecular (band-to-band) electron-hole recombination (with rate $k_2 n_{cc}$), and

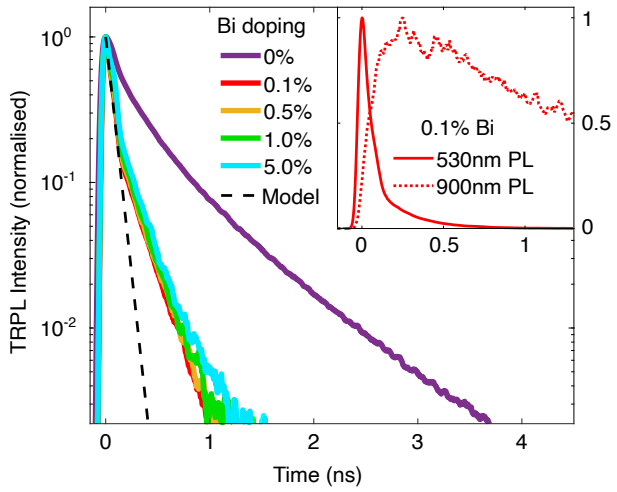

Figure 3: Time-resolved photoluminescence (TRPL) of bismuth-doped $MAPbBr_3$ thin films measured in vacuum with time-correlated single photon counting (TCSPC) setup, following a photoexcitation at 400 nm at a fluence of 40 nJ/cm^2. The decay traces are limited by the instrument response function of the detector, shown in the SI. The dotted black line represents the modelled PL decay as discussed in the main text. The inset shows a comparison of TRPL measured at 530 nm (band-edge) and 900 nm (sub-bandgap) for $MAPbBr_3$ doped with 0.1% Bi, shown on a linear vertical scale for clarity.

many-body (Auger) recombination ($k_3 n_{cc}^2$). However, as Auger recombination is a higher-order process, its contribution can often be neglected for hybrid perovskites when relatively low charge-carrier densities of $n_{cc} < 10^{20} cm^{-3}$ are employed (since for these densities, the rate $k_3 n_{cc}^2 << k_2 n_{cc}$ for typical values of k_2 and k_3 measured for lead-halide perovskites).[28–30] This condition is satisfied for the excitation fluences used in our study (since the highest used fluence of 17.5 $\mu J/cm^2$ corresponds to a photoexcited charge-carrier density of $\sim 10^{18}$ cm^{-3}) and we have therefore neglected Auger recombination in our analysis of the charge-carrier dynamics below.

Given that our above considerations suggest the occurrence of selective fast trapping of electrons in bismuth-doped $MAPbBr_3$ films, our model of the observed recombination dynamics needs to account for different rates of trap-mediated decays for photoexcited electrons and holes. In this case, the population densities of electrons (n) and holes (p) can be

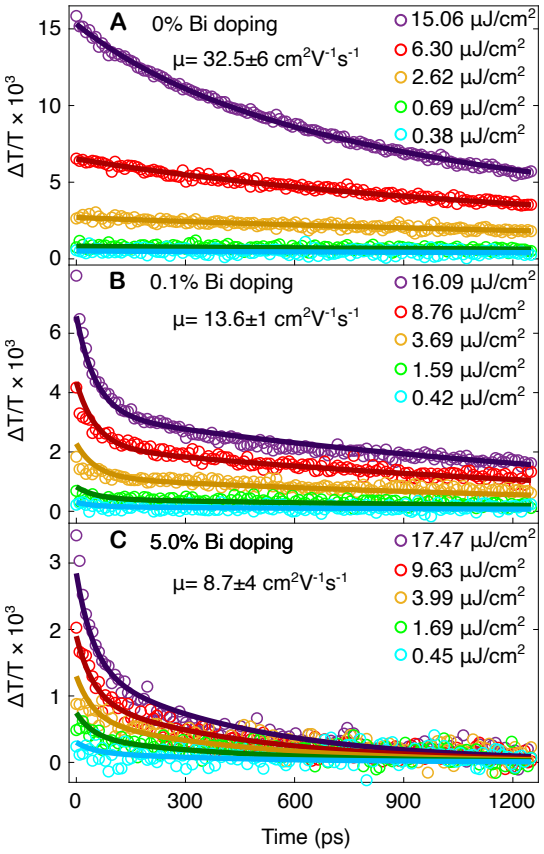

Figure 4: THz photoconductivity decays obtained from OPTP measurements in vacuum for Bi-doped $MAPbBr_3$ thin films. The data (hoops) for the (A) undoped (0% Bi doping) sample were globally fitted with a solution to Equation 3 (given by Equation S6 in the SI), as explained in the main text. Equation 9 (a bi-exponential decay) was used for the doped samples containing 0.1% (B) and 5% (C) bismuth doping. The fits are shown as solid lines. The indicated effective charge-carrier mobilities (μ) are extracted from the time = 0 onset of the photocoductivity and represent the sum of effective electron and hole mobilities. The indicated uncertainty is calculated from the standard deviation of the values recorded for different pump fluences. The full set of decay traces for all samples can be found in the SI.

described by the coupled differential equations:

$$\frac{\partial n}{\partial t} = -k_1^{\mathrm{e}} n - k_2 np \tag{1}$$

$$\frac{\partial p}{\partial t} = -k_1^{\mathrm{h}} p - k_2 np \tag{2}$$

where k_1^{e} and k_1^{h} are the trap-assisted recombination rates for electrons and holes, respectively, and k_2 is the bimolecular recombination rate constant. However, we can further simplify these equations for the two cases of undoped, and bismuth-doped $MAPbBr_3$, given that clear changes occur in the shape of the transients (see Figure 4) and their fluence dependence (Figure S3 in the SI) upon bismuth doping.

First, for the case of the undoped (0% Bi) $MAPbBr_3$ film the charge-carrier dynamics exhibit large fluence dependence (see Figure S3 in the SI for normalised curves), suggesting a significant contribution of bimolecular electron-hole recombination to the overall decay dynamics. Furthermore, at low pump fluences, the transients exhibit a monoexponential decay, indicating that the electron and hole monomolecular recombination constants can be approximated to be identical, $k_1^e = k_1^h = k_1$, resulting in Equations 1 and 2 being reduced to a single equation:

$$\frac{dn_{\mathrm{cc}}}{dt} = -k_1 n_{\mathrm{cc}} - k_2 n_{\mathrm{cc}}^2 \tag{3}$$

where $n_{\mathrm{cc}} = n = p$ is the charge-carrier population density of either electrons or holes. Figure 4 shows that fits to the photoconductivity ($\propto n_{\mathrm{cc}}$) transients of the undoped (0% Bi) $MAPbBr_3$ film (solid lines) based on this model (as explained in the SI), assuming global values of k_1 and k_2 across all fluences, provide an excellent match with the experimental data, confirming our assumptions of balanced electron and hole recombination rates.

Second, for the case of bismuth-doped $MAPbBr_3$ films, the charge-carrier dynamics exhibit very little dependence on excitation fluence (see Figure S3 in the SI), which indicates that trap-mediated (monomolecular) recombination now dominates over bimolecular recom-

bination pathways, in agreement with the observed severe suppression of the PL intensity for doped films (see Figures 2 and S1). In this case, the bimolecular recombination pathway can be neglected, simplifying Equations 1 and 2 to:

$$\frac{dn}{dt} = -k_1^{\mathrm{e}} n \tag{4}$$

$$\frac{dp}{dt} = -k_1^{\mathrm{h}} p \tag{5}$$

Equations 4 and 5 have simple monoexponential solutions for the charge-carrier populations, given by:

$$n = n_0 \exp(-k_1^{\mathrm{e}} t) \tag{6}$$

$$p = n_0 \exp(-k_1^{\mathrm{h}} t) \tag{7}$$

where n_0 is the initial number of electron-hole pairs straight after photoexcitation. Within the simple Drude model, the electron-hole sum photoconductivity σ determined in the OPTP measurements[6] is equal to the sum of the individual products of electron and hole population densities and their respective mobilities:

$$\sigma(t) = \mu_{\mathrm{e}} n(t) e + \mu_{\mathrm{h}} p(t) e \tag{8}$$

where μ_{e} and μ_{h} are the mobilities of electrons and holes respectively, assumed to be unchanged over the timescales of the measurements. Equations 6, 7 and 8 thus imply a bi-exponential decay of the THz photoconductivity in the case of bismuth-doped $MAPbBr_3$ thin films:

$$\sigma(t) = n_0 e[\mu_{\mathrm{e}} \exp\left(-k_1^{\mathrm{e}} t\right) + \mu_{\mathrm{h}} \exp\left(-k_1^{\mathrm{h}} t\right)] \tag{9}$$

As Figure S3 in the SI illustrates, the photoconductivity in bismuth-doped films indeed deviates from a simple monoexponential behaviour, even at low pump fluences, showing that doping leads to imbalanced electron and hole decay dynamics, through an enhancement of

selective, ultrafast electron trapping. This selective trapping, together with slow recombination dynamics with free holes manifest itself in bi-exponential photoconductivity decays. We note, however, that the shape of the photoconductivity transients significantly differs from that observed for time-resolved band-edge PL decays. This difference originates from the fact that while the photoconductivity measurement is sensitive to the sum of the contributions of electron and hole populations (whose different decay rates result in bi-exponential photoconductivity decay), the band-edge PL originates from the radiative recombination of free electrons with holes. Therefore, the PL intensity I_{PL} is proportional to the product of electron and hole populations, which, even for imbalanced trapping, results in monoexponential PL intensity transients with rate equal to the sum of the individual decay rates of electrons and holes ($k_1^{\mathrm{e}} + k_1^{\mathrm{h}}$):

$$I_{\mathrm{PL}}(t) \propto k_2 n(t) p(t) = k_2 \exp\left(-[k_1^{\mathrm{e}} + k_1^{\mathrm{h}}]t\right). \tag{10}$$

To probe the validity of the fast, selective trapping model for bismuth-doped $MAPbBr_3$ thin films, we first fitted the OPTP photoconductivity transients with Eqn. 9 in order to obtain the decay constants k_1^{e} and k_1^{h}, then used these to validate that they also accurately reflected the PL dynamics according to Eqn. 10. Figure 4 B and C shows excellent agreement between the selective trapping model and the photoconductivity data, which reflects the strongly bi-exponential decay of the photoconductivity according to Equation 9. Values for the extracted decay constants k_1^{e} and k_1^{h} have been plotted against the percentage of bismuth doping in Figure 5. The faster decay component was assigned to the rapid trapping of electrons (k_1^e), based on existing literature investigating the nature of native defects in undoped $MAPbBr_3$ thin films.[26] We then ascertained that these extracted monomolecular rate constants are consistent with the time-resolved photoluminescence transients shown in Figure 3. For this purpose, the dotted black line in Figure 3 represents the expected decay of the PL signal for the doped films, as calculated from Equation 10 using the monomolec-

ular constants extracted from OPTP data. We note that this predicted PL decay generally reflects the data well, but is slightly faster because the TCSPC measurements are limited by the instrument response of our detector (sub-nanosecond, as shown in Figure S2 the SI). Our observations of the temporal behaviour of the photoconductivity as well as the photoluminescence in doped and undoped $MAPbBr_3$ thin films thus support the notion that bismuth doping enhances selective trapping of one charge-carrier species following photoexcitation. Such fast electron trapping leads to an initial rapid decrease of the photoconductivity ($\propto [\mu_e n + \mu_h p]$), which subsequently decays slowly due to hole trapping as well as recombination of trapped electrons with free holes. These effects together lead, however, to a rapid quenching of PL intensity ($\propto k_2 pn$).

The OPTP photoconductivity measurements not only allow us to investigate the dynamics of charge-carrier populations but also their mobilities, since the photoconductivity of the thin film depends on the product of these two quantities. By estimating the initial density of charge-carrier pairs n_0, we are able to obtain the sum of the electron and hole mobilities from the onset of the photoconductivity at time $t = 0$, according to Equation 9. Here, the initial density n_0 is determined from the absorption of the films at the excitation wavelength, under the assumption that each absorbed photon photoexcites one electron-hole pair.[6] Figure 5 displays the extracted values of the electron-hole sum mobilities. We observe a significant decrease of charge-carrier mobility with bismuth doping, which we attribute to an increased presence of charged defects in the doped films that enhance the scattering rate of charge carriers. We note that this reduction of charge-carrier mobility correlates with the observed broadening of the absorption spectra discussed earlier (see Figure 5 A&B), which is expected, given that the presence of charged defects will also lead to additional energetic disorder in the bismuth-doped perovskite films.

In addition, we find that our photoconductivity transients of the doped perovskite films also permit us to deduce the ratio of electron to hole mobilities, by exploiting the different dynamics of the photoexcited charge-carrier species. As Equation 9 shows, this electron-

hole mobility ratio is determined by the relative amplitudes of the two monoexponential decay components of the individual carrier species that comprise the overall bi-exponential photoconductivity transient. To obtain an accurate value for the mobility ratio we performed a globally optimised fitting procedure for transients recorded for all the doped samples and excitation fluences as outlined in the SI. We determined a ratio of $\frac{\mu_e}{\mu_h} = 1.0 \pm 0.2$, indicating highly balanced electron and hole mobilities in $MAPbBr_3$ with relatively strong experimental accuracy. We note that a value of $\frac{\mu_e}{\mu_h} = 1$ has been therefore used for all fits to the presented OPTP transients of the doped perovskites. To put these findings into context we note that, for lead-halide perovskites, numerous theoretical calculations indicate similarity of electron and hole effective masses,[31–35] implying balanced mobilities under the assumption that scattering rates for the charge carriers are also similar. Thus, our findings provide experimental evidence that bromide perovskites exhibit balanced mobilities, which, together with existing calculations on their masses, suggests that scattering rates are also similar for the two species.

Overall, based on our observations, we deduce that bismuth doping increases the density of point defect states in thin films of $MAPbBr_3$ perovskites. These defects trap the majority of photoexcited electrons on ultrafast timescales (10^{-10} s) and act as scattering centres for the photoexcited charge carriers, reducing their lifetimes and mobilities. Unfortunately, bismuth also cannot be used as a tool for bandgap engineering in these materials, as its presence affects neither the exciton binding energy nor the bandgap energy of the semiconductor. These conclusions can be drawn from our observations summarised in Figure 5, which shows an increase of the absorption edge broadening (Γ) indicating enhanced energetic disorder in the films and a decrease of charge-carrier mobility (μ), originating from higher scattering rates from defects with increasing bismuth doping of $MAPbBr_3$. The exciton binding energy (E_b) and bandgap of the semiconductors remain unaffected by doping. The trap-assisted recombination rates for electrons (k_1^e) and holes (k_1^h) increase sharply upon doping $MAPbBr_3$ even when a small amount (0.1%) of the chemical dopant is used. We

note that upon further increase of doping level, k_1^e and k_1^h do not rise significantly more, indicating that the number of defects introduced into the films is not directly proportional to the amount of dopant added. Since Abdelhady et al. have shown that the number of Bi ions incorporated into the crystalline structure of the perovskite grows linearly with the concentration of added $BiBr_3$ salt,[10] we suspect that the heterovalent ions are not directly acting as electron-trapping defects. We rather propose that a halide excess associated with $BiBr_3$ addition leads to an enhancement of bromide interstitial formation. These halide interstitials have been shown by Motti et al.[26] to trap electrons on ultrafast timescales and to result in weak IR emission caused by slow recombination of trapped electrons with free holes, even in undoped $MAPbBr_3$ perovskites. Because the IR emission in our undoped $MAPbBr_3$ film has the same spectral shape as the sub-bandgap PL in the doped films, we suggest that these native halide interstitials are responsible for enhanced electron trapping observed in bismuth-doped perovskites, resulting in the observed bi-exponential decay of the photoconductivity, quenching of steady-state PL intensity and time-resolved PL lifetimes and significant enhancement of IR photoluminescence. Although we cannot definitively exclude the possibility of bismuth ions forming new defect states of similar energy,[16] we believe our data provides strong evidence that the deterioration is instead caused by an associated presence of halide interstitials.

Finally, we comment on the question of the influence of structural disorder on increasing the charge-carrier recombination rates in Bi-doped perovskites, which still has not been answered in the literature.[11,14,15,17,18] We find that both the crystallinity of the films and the lattice constant of the perovskite crystals remain unaltered upon bismuth doping of $MAPbBr_3$. Our analysis of the XRD spectra of the films reveal no broadening or shifts of the diffraction peaks when bismuth is added (see Figures S6–S8 in the SI). Moreover, the optical phonon modes of the lead-bromide lattice remain unaffected by doping, as can be seen from THz dark conductivity measurement shown in Figure S9 in the SI. These data suggest that bismuth doping induces few structural changes, and the observed energetic

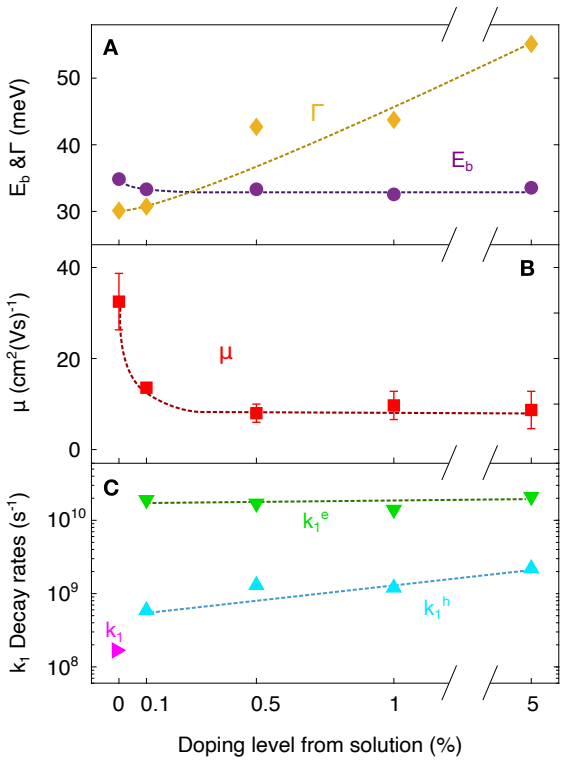

Figure 5: Dependence of structural and dynamical parameters on Bi doping of $MAPbBr_3$ thin films. (A) Broadening of the absorption spectrum Γ (yellow diamonds) and the exciton binding energy E_b (purple circles), obtained from fits of the Elliott model to FTIR absorption spectra. (B) Electron-hole sum mobility μ (red squares), extracted from the initial value of the photoconductivity. The error corresponds to the standard deviation of the values obtained for different excitation fluences. (C) Monomolecular decay rates extracted from fits to the OPTP transients. For the undoped $MAPbBr_3$ films, a single value of k_1 (magenta right-pointing triangle) was extracted for both electrons and holes, based on the fits of Equation S6 (shown in the SI) to the OPTP transients. For bismuth-doped $MAPbBr_3$ films, decay rates k_1^e (blue up-pointing triangle) and k_1^h (green down-pointing triangle) were extracted from fits of a bi-exponential function according to Equation 9. The monomolecular decay rates k_1^e and k_1^h were assigned to initial fast trapping of electrons and slow decay of photoexcited holes population respectively. Dotted lines are a guide to the eye only.

broadening and accelerated charge-carrier decay must instead derive from an introduction of point defect states into the perovskite films.

In conclusion, we have investigated the effect of bismuth doping on thin films of $MAPbBr_3$ perovskite. As the thin film technology is commonly used in solar cell devices, our results are directly relevant to the rapidly evolving field of perovskite photovoltaics and light-emitting applications. The initial reports of successful bismuth incorporation into perovskites indicated that bismuth doping can improve the properties of the semiconductor[12,13] and could be used as a tool for bandgap tuning in $MAPbBr_3$ crystals.[10] However, we have found that the addition of bismuth to the $MAPbBr_3$ thin films increases the energetic disorder in these semiconductors, without affecting the bandgap, exciton binding energy or structural properties of the crystal. Bismuth doping also lowers charge-carrier mobilities and increases monomolecular recombination rates, which in turn decreases the charge-carrier diffusion length. Such effects are potentially detrimental to the performance of the perovskite layer, raising concerns over the use of bismuth for PV applications.

Although our results present bismuth-doped $MAPbBr_3$ as a poorly performing material for the absorption layer in solar cells, they also provide valuable insights into the mechanism of charge-carrier trapping in these semiconductors. This understanding may lead to a performance improvement of doped perovskites used in photovoltaics. As the main route of charge-carrier recombination in Bi-doped $MAPbBr_3$ is through a selective trapping of electrons, reducing the density of the point defects could result in prolonged charge-carrier lifetimes, enhanced charge-carrier mobilities and diffusion lengths. Such an improvement of the optoelectronic properties of Bi-doped perovskites, together with previously reported stability and doping-induced rise of conductivity, would make bismuth a potentially interesting additive. Therefore, it is important to find additional agents to prevent the formation of point defects, such as halide interstitials, in these materials. We note in this context that all recent studies used the addition of $BiBr_3$ salt to the precursor solution as a route of bismuth doping,[10–12,14,15] which, as suggested by Abdelhady et al.,[10] results in a controlled incorpo-

ration of Bi into the perovskite crystal. However, since this method results in a bromide excess during deposition, we propose that other ways of Bi doping should be investigated to avoid the potential enhancement of bromide interstitial formation. Different heterovalent doping schemes should also be investigated in order to identify dopants that do not reduce the optoelectronic performance – as for example $Ce_3{}^+$ used in inorganic perovskites[36] or SnF_2 for tin perovskites.[28] Overall, our study provides a framework for the analysis of doping effects in hybrid perovskites, which will further the assessment of such schemes for tuning the optoelectronic properties of the active layer in perovskite solar cells.

Acknowledgement

The authors acknowledge financial support from Engineering and Physical Sciences Research Council (EPSRC), UK., through research grant funding, and a Prosperity Partnership. A.M.U. also thanks EPSRC Centre for Doctoral Training (CDT) for Science and Applications of Plastic Electronic Materials for financial support through a graduate studentship. J.B. thanks the EPSRC CDT for New and Sustainable Photovoltaics for financial support through a graduate studentship. L.M.H. and M.B.J. acknowledge support from the Alexander-von-Humboldt foundation through research awards.

Supporting Information Available

Experimental details and sample fabrication method, details of fits based on Elliott Theory, additional steady-state photoluminescence spectra, THz photoconductivity traces and details of decay modelling, determination of electron-hole mobility ratio, X-ray diffraction patterns and dark THz conductivity spectra of bismuth-doped $MAPbBr_3$ films.

References

(1) National Renewable Energy Laboratory, NREL Efficiency Chart (accessed Mar 09, 2020).

(2) D'innocenzo, V.; Grancini, G.; Alcocer, M. J.; Kandada, A. R. S.; Stranks, S. D.; Lee, M. M.; Lanzani, G.; Snaith, H. J.; Petrozza, A. Excitons versus free charges in organo-lead tri-halide perovskites. *Nature Communications* **2014**, *5*, 3586.

(3) Galkowski, K.; Mitioglu, A.; Miyata, A.; Plochocka, P.; Portugall, O.; Eperon, G. E.; Wang, J. T.-W.; Stergiopoulos, T.; Stranks, S. D.; Snaith, H. J. et al. Determination of the exciton binding energy and effective masses for methylammonium and formamidinium lead tri-halide perovskite semiconductors. *Energy & Environmental Science* **2016**, *9*, 962–970.

(4) Miyata, A.; Mitioglu, A.; Plochocka, P.; Portugall, O.; Wang, J. T.-W.; Stranks, S. D.; Snaith, H. J.; Nicholas, R. J. Direct measurement of the exciton binding energy and effective masses for charge carriers in organic–inorganic tri-halide perovskites. *Nature Physics* **2015**, *11*, 582.

(5) Ponseca Jr, C. S.; Savenije, T. J.; Abdellah, M.; Zheng, K.; Yartsev, A.; Pascher, T.; Harlang, T.; Chabera, P.; Pullerits, T.; Stepanov, A. et al. Organometal halide perovskite solar cell materials rationalized: ultrafast charge generation, high and microsecond-long balanced mobilities, and slow recombination. *Journal of the American Chemical Society* **2014**, *136*, 5189–5192.

(6) Wehrenfennig, C.; Liu, M.; Snaith, H. J.; Johnston, M. B.; Herz, L. M. Charge-carrier dynamics in vapour-deposited films of the organolead halide perovskite $CH_3NH_3PbI_{3-x}Cl_x$. *Energy & Environmental Science* **2014**, *7*, 2269–2275.

(7) Johnston, M. B.; Herz, L. M. Hybrid perovskites for photovoltaics: charge-carrier re-

combination, diffusion, and radiative efficiencies. *Accounts of Chemical Research* **2015**, *49*, 146–154.

(8) Meggiolaro, D.; Motti, S. G.; Mosconi, E.; Barker, A. J.; Ball, J.; Perini, C. A. R.; Deschler, F.; Petrozza, A.; De Angelis, F. Iodine chemistry determines the defect tolerance of lead-halide perovskites. *Energy & Environmental Science* **2018**, *11*, 702–713.

(9) Noh, J. H.; Im, S. H.; Heo, J. H.; Mandal, T. N.; Seok, S. I. Chemical management for colorful, efficient, and stable inorganic–organic hybrid nanostructured solar cells. *Nano Letters* **2013**, *13*, 1764–1769.

(10) Abdelhady, A. L.; Saidaminov, M. I.; Murali, B.; Adinolfi, V.; Voznyy, O.; Katsiev, K.; Alarousu, E.; Comin, R.; Dursun, I.; Sinatra, L. et al. Heterovalent dopant incorporation for bandgap and type engineering of perovskite crystals. *The Journal of Physical Chemistry Letters* **2016**, *7*, 295–301.

(11) Meng, R.; Wu, G.; Zhou, J.; Zhou, H.; Fang, H.; Loi, M. A.; Zhang, Y. Understanding the Impact of Bismuth Heterovalent Doping on the Structural and Photophysical Properties of $CH_3NH_3PbBr_3$ Halide Perovskite Crystals with Near-IR Photoluminescence. *Chemistry–A European Journal* **2019**, *25*, 5480–5488.

(12) Han, L.; Wu, L.; Liu, C.; Zhang, J. Doping-Enhanced Visible-Light Absorption of $CH_3NH_3PbBr_3$ by the Bi^{3+}-Induced Impurity Band without Sacrificing a Band gap. *The Journal of Physical Chemistry C* **2019**, *123*, 8578–8587.

(13) Hu, Y.; Bai, F.; Liu, X.; Ji, Q.; Miao, X.; Qiu, T.; Zhang, S. Bismuth incorporation stabilized α-$CsPbI_3$ for fully inorganic perovskite solar cells. *ACS Energy Letters* **2017**, *2*, 2219–2227.

(14) Nayak, P. K.; Sendner, M.; Wenger, B.; Wang, Z.; Sharma, K.; Ramadan, A. J.; Lovrincic, R.; Pucci, A.; Madhu, P.; Snaith, H. J. Impact of Bi^{3+} heterovalent doping in

organic–inorganic metal halide perovskite crystals. *Journal of the American Chemical Society* **2018**, *140*, 574–577.

(15) Yamada, Y.; Hoyano, M.; Oto, K.; Kanemitsu, Y. Effects of Impurity Doping on Photoluminescence Properties of $APbX_3$ Lead Halide Perovskites. *Physica Status Solidi (b)* **2019**, 1800545.

(16) Li, J.-L.; Yang, J.; Wu, T.; Wei, S.-H. Formation of DY center as n-type limiting defects in octahedral semiconductors: the case of Bi-doped hybrid halide perovskites. *Journal of Materials Chemistry C* **2019**, *7*, 4230–4234.

(17) Yavari, M.; Ebadi, F.; Meloni, S.; Wang, Z. S.; Yang, T. C.-J.; Sun, S.; Schwartz, H.; Wang, Z.; Niesen, B.; Durantini, J. et al. How far does the defect tolerance of lead-halide perovskites range? The example of Bi impurities introducing efficient recombination centers. *Journal of Materials Chemistry A* **2019**,

(18) Yamada, Y.; Hoyano, M.; Akashi, R.; Oto, K.; Kanemitsu, Y. Impact of chemical doping on optical responses in bismuth-doped $CH_3NH_3PbBr_3$ single crystals: carrier lifetime and photon recycling. *The Journal of Physical Chemistry Letters* **2017**, *8*, 5798–5803.

(19) Lozhkina, O. A.; Murashkina, A. A.; Shilovskikh, V. V.; Kapitonov, Y. V.; Ryabchuk, V. K.; Emeline, A. V.; Miyasaka, T. Invalidity of Band-Gap Engineering Concept for Bi^{3+} Heterovalent Doping in $CsPbBr_3$ Halide Perovskite. *The Journal of Physical Chemistry Letters* **2018**, *9*, 5408–5411.

(20) Elliott, R. Intensity of optical absorption by excitons. *Physical Review* **1957**, *108*, 1384.

(21) Davies, C. L.; Filip, M. R.; Patel, J. B.; Crothers, T. W.; Verdi, C.; Wright, A. D.; Milot, R. L.; Giustino, F.; Johnston, M. B.; Herz, L. M. Bimolecular recombination in methylammonium lead triiodide perovskite is an inverse absorption process. *Nature Communications* **2018**, *9*, 293.

(22) Wehrenfennig, C.; Liu, M.; Snaith, H. J.; Johnston, M. B.; Herz, L. M. Homogeneous emission line broadening in the organo lead halide perovskite $CH_3NH_3PbI_{3-x}Cl_x$. *The Journal of Physical Chemistry Letters* **2014**, *5*, 1300–1306.

(23) Wright, A. D.; Verdi, C.; Milot, R. L.; Eperon, G. E.; Pérez-Osorio, M. A.; Snaith, H. J.; Giustino, F.; Johnston, M. B.; Herz, L. M. Electron–phonon coupling in hybrid lead halide perovskites. *Nature Communications* **2016**, *7*, 11755.

(24) Sestu, N.; Cadelano, M.; Sarritzu, V.; Chen, F.; Marongiu, D.; Piras, R.; Mainas, M.; Quochi, F.; Saba, M.; Mura, A. et al. Absorption F-sum rule for the exciton binding energy in methylammonium lead halide perovskites. *The Journal of Physical Chemistry Letters* **2015**, *6*, 4566–4572.

(25) Crothers, T. W.; Milot, R. L.; Patel, J. B.; Parrott, E. S.; Schlipf, J.; Muller-Buschbaum, P.; Johnston, M. B.; Herz, L. M. Photon reabsorption masks intrinsic bimolecular charge-carrier recombination in $CH_3NH_3PbI_3$ perovskite. *Nano Letters* **2017**, *17*, 5782–5789.

(26) Motti, S. G.; Meggiolaro, D.; Martani, S.; Sorrentino, R.; Barker, A. J.; De Angelis, F.; Petrozza, A. Defect Activity in Lead Halide Perovskites. *Advanced Materials* **2019**, *31*, 1901183.

(27) Herz, L. M. Charge-carrier dynamics in organic-inorganic metal halide perovskites. *Annual Review of Physical Chemistry* **2016**, *67*, 65–89.

(28) Milot, R. L.; Klug, M. T.; Davies, C. L.; Wang, Z.; Kraus, H.; Snaith, H. J.; Johnston, M. B.; Herz, L. M. The effects of doping density and temperature on the optoelectronic properties of formamidinium tin triiodide thin films. *Advanced Materials* **2018**, *30*, 1804506.

(29) Milot, R. L.; Eperon, G. E.; Green, T.; Snaith, H. J.; Johnston, M. B.; Herz, L. M. Radiative monomolecular recombination boosts amplified spontaneous emission in

$HC(NH_2)_2SnI_3$ perovskite films. *The Journal of Physical Chemistry Letters* **2016**, *7*, 4178–4184.

(30) Noel, N. K.; Stranks, S. D.; Abate, A.; Wehrenfennig, C.; Guarnera, S.; Haghighirad, A.-A.; Sadhanala, A.; Eperon, G. E.; Pathak, S. K.; Johnston, M. B. et al. Lead-free organic–inorganic tin halide perovskites for photovoltaic applications. *Energy & Environmental Science* **2014**, *7*, 3061–3068.

(31) Feng, J.; Xiao, B. Crystal structures, optical properties, and effective mass tensors of $CH_3NH_3PbX_3$ (X= I and Br) phases predicted from HSE06. *The Journal of Physical Chemistry Letters* **2014**, *5*, 1278–1282.

(32) Chang, Y.; Park, C. H.; Matsuishi, K. First-principles study of the Structural and the electronic properties of the lead-halide-based inorganic-organic perovskites $(CH_3NH_3)PbX_3$ and $CsPbX_3$ (X= Cl, Br, I). *Journal of the Korean Physical Society* **2004**, *44*, 889–893.

(33) Melissen, S. T. A. G.; Labat, F.; Sautet, P.; Le Bahers, T. Electronic properties of $PbX_3CH_3NH_3$ (X = Cl, Br, I) compounds for photovoltaic and photocatalytic applications. *Physical Chemistry Chemical Physics* **2015**, *17*, 2199–2209.

(34) Protesescu, L.; Yakunin, S.; Bodnarchuk, M. I.; Krieg, F.; Caputo, R.; Hendon, C. H.; Yang, R. X.; Walsh, A.; Kovalenko, M. V. Nanocrystals of cesium lead halide perovskites ($CsPbX_3$, X= Cl, Br, and I): novel optoelectronic materials showing bright emission with wide color gamut. *Nano Letters* **2015**, *15*, 3692–3696.

(35) Akkerman, Q. A.; Motti, S. G.; Srimath Kandada, A. R.; Mosconi, E.; D'Innocenzo, V.; Bertoni, G.; Marras, S.; Kamino, B. A.; Miranda, L.; De Angelis, F. et al. Solution synthesis approach to colloidal cesium lead halide perovskite nanoplatelets with monolayer-level thickness control. *Journal of the American Chemical Society* **2016**, *138*, 1010–1016.

(36) Yao, J.-S.; Ge, J.; Han, B.-N.; Wang, K.-H.; Yao, H.-B.; Yu, H.-L.; Li, J.-H.; Zhu, B.-S.; Song, J.-Z.; Chen, C. et al. Ce^{3+}-doping to modulate photoluminescence kinetics for efficient $CsPbBr_3$ nanocrystals based light-emitting diodes. *Journal of the American Chemical Society* **2018**, *140*, 3626–3634.